JACS
JOURNAL OF THE AMERICAN CHEMICAL SOCIETY

ARTICLE

pubs.acs.org/JACS

Mechanical Unfolding of the Beet Western Yellow Virus −1 Frameshift Signal

Katherine H. White,[†] Marek Orzechowski,[*,‡] Dominique Fourmy,[§] and Koen Visscher[*,∥]

[†]Department of Chemistry and Biochemistry and [∥]Departments of Physics and Molecular & Cellular Biology and the College of Optical Sciences, University of Arizona, Tucson, Arizona 85721, United States

[‡]Department of Physiology and Biophysics, Boston University, Boston, Massachusetts 02215, United States

[§]Centre de Génétique Moléculaire CGM-CNRS, 91198 Gif-sur-Yvette, France

Supporting Information

ABSTRACT: Using mechanical unfolding by optical tweezers (OT) and steered molecular dynamics (SMD) simulations, we have demonstrated the critical role of Mg^{2+} ions for the resistance of the Beet Western Yellow Virus (BWYV) pseudoknot (PK) to unfolding. The two techniques were found to be complementary, providing information at different levels of molecular scale. Findings from the OT experiments indicated a critical role of stem 1 for unfolding of the PK, which was confirmed in the SMD simulations. The unfolding pathways of wild type and mutant appeared to depend upon pH and nucleotide sequence. SMD simulations support the notion that the stability of stem 1 is critical for −1 frameshifting. The all-atom scale nature of the SMD enabled clarification of the precise role of two Mg^{2+} ions, Mg45 and Mg52, as identified in the BWYV X-ray crystallography structure, in −1 frameshifting. On the basis of simulations with "partially" and "fully" hydrated Mg^{2+} ions, two possible mechanisms of stabilizing stem 1 are proposed. In both these cases Mg^{2+} ions play a critical role in stabilizing stem 1, either by directly forming a salt bridge between the strands of stem 1 or by stabilizing parallel orientation of the strands in stem 1, respectively. These findings explain the unexpected drop in frameshifting efficiency to null levels of the C8U mutant in a manner consistent with experimental observations.

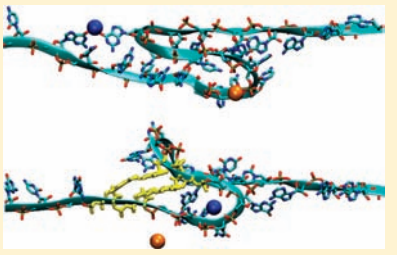

INTRODUCTION

The Beet Western Yellow Virus (BWYV) belongs to the family of plant luteoviruses regulating the expression of its RNA-dependent RNA polymerase by programmed −1 frameshifting (−1FS) in a fashion identical to the well-known *gag*−*pol* retroviral frameshifting (FS).[1−4] Translational recoding by −1FS occurs in response to a specific downstream mRNA structure, usually a pseudoknot (PK), which resists unwinding while the ribosome is paused over a "slippery sequence".[5,6] Tension is built up as the PK resists unfolding, disrupting the codon−anticodon interactions and relieving the tension when they are restored in the −1 reading frame.[7−9] The FS efficiency, measured as the probability of FS to occur, depends upon the nucleotide sequence of the slippery sequence,[10] the stability of the downstream structure,[11,12] and the short mRNA spacer sequence connecting the two.[10,13]

The BWYV PK (with slippery sequence G GGA AAC) yields a FS efficiency of up to 10.8% depending upon in vivo or in vitro conditions.[12] The BWYV PK has a remarkably small (26 nucleotides) and compact structure.[14−16] Compared to most other H-type PKs, the loop−stem tertiary structural interactions in the BWYV PK are extensive: the number of tertiary hydrogen-bonding interactions, 26, exceeds the number of hydrogen bonds in Watson−Crick base pairs, 24.[14−16] This is consistent with results of thermal melting experiments, which indicate that the PK is stabilized by an enthalpic component that greatly exceeds that of other H-type and frameshifting PKs for which secondary structure accounts for nearly all of the folding enthalpy.[17]

The BWYV PK is characterized by two helical stems, 1 and 2, connected by two loops, 1 and 2.[16] The helical stems are not coaxially stacked as in other H-type PKs, due to the 48° rotation between A25 in stem 2 and G7 in stem 1, which causes an approximate 5 Å helical displacement of the stems with respect to each other.[16] There also is a 25° kink at the junction between stem 1 and loop 2.[16] Interestingly, U13 does not base-pair with A25 as part of stem 2, as one would expect, but rather bulges out while A25 is stacked on loop 2.[15]

A cytosine in position 8 is a member of a quadruple base interaction involving the G12-C26 base pair from stem 2 as well as A25, the linker between stem 2 and the stem 1−loop 2 triplex.[15] While loop 1 of the PK crosses the major groove of stem 2, C8 is the only member of loop 1 that is positioned in a sufficient orientation to form hydrogen bonds with G12 and C26.[15] Since the quadruple-base interaction holds together nucleotides from loop 1, stem 2, and the stem 1−loop 2 triplex, it is thought that the C8-coordinated region may influence the equilibrium between folded and unfolded forms of the PK.[12] Protonation of C8 as well as its orientation allows for the

Received: December 14, 2010
Published: May 20, 2011

dx.doi.org/10.1021/ja111281f | *J. Am. Chem. Soc.* 2011, 133, 9775–9782

formation of more hydrogen bonds than would be predicted from normal, Watson−Crick base pairing.[15]

Mutating C8 to any other base reduces the FS efficiency to background levels.[12] The C8A mutation disrupts the unique setup created by C8 both sterically and by reducing the number of favorable hydrogen-bonding contacts. A more surprising result is that a C8U mutation causes a complete loss of frameshifting but presumably only changes the environment by removing one hydrogen bond between the N(4)-H of C8 and N(7) of G12.

Several metal ions have been observed in the crystal structure of the BWYV PK.[14] Four Na^+ ions have been identified, with two residing adjacent to the stem 1−loop 2 junction and thought to be important for PK stability.[14] Thermal melting data yields the sensitivity of tertiary interactions on monovalent ion concentrations but is independent of the type of ion, Na^+, K, or NH_4^+.[17] Two Mg^{2+} ions (Mg45 and Mg52) reside in the major groove of stem 1, and one (Mg38) resides in the major groove of stem 2.[14] Mg45 occupies a key site in the structure, whereas the roles of Mg52 and Mg38 are not as obvious. Mg45 is coordinated at the upper end of stem 1, near the bulged-out U13, at the stem 1−stem 2 interface.

Our goal was to investigate stability of BYWV PK and its resistance to unfolding as a determining factor for −1FS efficiency. Experimental (optical tweezers, OT) and computational (steered molecular dynamics, SMD) techniques were combined to study the influence of Mg^{2+} ions and various mutations of residue C8 on the resistance of the PK to unfolding. We note that comparison of the results of either method can only be qualitative due to the large difference in the pulling speeds (see Materials and Methods).

MATERIALS AND METHODS

Unfolding with Optical Tweezers. Individual BWYV PK structures sandwiched between two hybrid DNA/RNA handles[18] were stretched and unfolded by use of OT. One handle was attached to a microscope cover slide glass surface via a biotin−streptavidin interaction, whereas the other handle, end-labeled with digoxigenin, was linked to an anti-dig-coated polystyrene microsphere. Force−extension data were then obtained by laterally moving the piezo-driven microscope stage while simultaneously recording the position of the microsphere in the OT. The increase in contour length (number of nucleotides) upon unfolding of the PK was computed by use of a wormlike chain model for polymer elasticity; we assumed a stretching modulus of 1000 pN, a persistence length of 1 nm, an interphosphate distance of 0.59 nm and we estimated a stem thickness of 2 nm.[19,20] Molecules were stretched in 10 mM Tris buffer, 125 mM NaCl, and 2 mg/mL bovine serum albumin (BSA), with pH and Mg^{2+} concentrations adjusted to desired values. Pulling speeds were approximately 20 nm/s. See the Supporting Information and ref 20 for further details.

Unfolding with Steered Molecular Dynamics. In order to perform unfolding of the BWYV PK with all-atom resolution, steered molecular dynamics (SMD) was used.[21] All of the simulations were carried out with the NAMD program[22] using the parm99bsc0[23] modification of the parm99 force−field[24−26] of the Amber package.[27] Nonbonded van der Waals (vdW) parameters for the ions were based on the work of Aaqvist.[28] As a model system we used the high-resolution structure of the BWYV PK, obtained in the presence of monovalent and divalent ions by Egli et al.[14] (PDB ID 1L2X). This PK structure consists of 28 nucleotides with sequence 5′-GGCGCGGCACCGUCCGCG-GAACAAACGG-3′ as used in the OT experiments (Figure 1C,F). The first two residues, G1 and G2, are not present in the native PK. In the setup for the simulations, G1 residue was removed, whereas G2 was left to act as a buffer for the external force applied to stretch the PK. All of the ions present in the crystal structure (6 Mg^{2+}, 3 Na^+, 1 K^+) were left in their original positions. By use of the LEap program, an additional minimal set of sodium ions was added

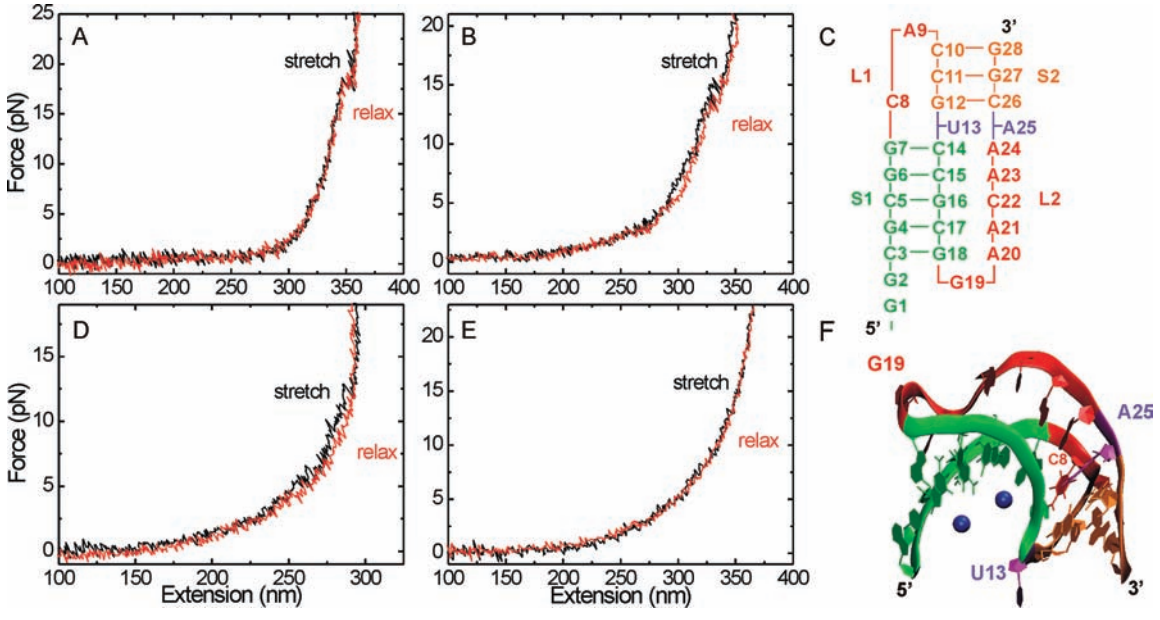

Figure 1. Force−extension data for the WT BWYV pseudoknot when stretched with optical tweezers (250 mM NaCl and 5 mM $MgCl_2$). (A) Typical near-equilibrium behavior with rapid unfolding and refolding ("hopping"), which occurs 93% of the time at pH = 7.3. (B) Typical near-equilibrium behavior as it occurred 58% of the time at pH = 6.3. (C) BWYV PK sequence and secondary structure. L1 and L2 = loops 1 and 2; S1 and S2 = stems and 1 and 2. (D) Typical off-equilibrium behavior that occurs the remaining 42% of the time at pH = 6.3. (E) In the absence of Mg^{2+}, the force−extension data do not exhibit any unfolding transitions. (F) BWYV PK structure—color coding shared with panel C. Blue spheres depict Mg^{2+} ions.

dx.doi.org/10.1021/ja111281f |J. Am. Chem. Soc. 2011, 133, 9775–9782

to neutralize the system. In the case of the PK with protonated C8, nine sodium ions were added, whereas in all the other systems 10 sodium ions were added. The additional ions were placed at points of electrostatically favorable potential around the PK. The minimal set of counterions was used similarly to the original work of Pérez et al.,[23] who tested parmbsc0 parameters in MD simulations. This approach has been validated in various MD simulations of nucleic acids.[24,25,29,30]

In the crystal structure, the Mg^{2+} ions are fully hydrated; that is, they have a complete octahedral hydration shell. In the initial setup, all the water molecules present in the crystal structure were removed and the PK, together with all the ions from the X-ray structure, was solvated with a box of randomly distributed water molecules. After minimization, 4 Mg^{2+} ions were found to quickly associate and directly interact with nucleic acid bases (one ion: Mg52) or the backbone's phosphate groups (three ions: Mg34, Mg38, and Mg45). As a result, one or two water molecules from the first hydration shell were replaced by the aforementioned PK's atoms. Further heating and equilibration did not restore the full hydration of these Mg^{2+} ions, and we will refer to these simulations as partially hydrated Mg^{2+} ions setup.

Experimental studies suggest that the octahedral complexes of Mg^{2+} ions with water are stable, so that any spontaneous exchange of water ligands in the first hydration layer of Mg^{2+} occurs slowly, at time scales on the order of 10^{-5}–10^{-6} s.[31] On the other hand, analysis of the PDB database[32] as well as results from computational approaches, such as ab initio calculations,[33,34] suggest that direct interactions between partially hydrated Mg^{2+} ions and nucleic acids cannot be ignored and should be considered. Therefore, in order to study direct interactions between Mg^{2+} and the PK, we had to initiate simulations with partially hydrated Mg^{2+} ions because spontaneous water ligand exchange would be too slow and beyond the capabilities of our atomic-scale MD simulations. Upon initial inspection of the crystallographic structure, direct interactions between one of the Mg^{2+} ions with two highly electronegative O6 atoms in guanines G4 and G16 can readily occur, without disruption of the octahedral conformation of the coordinated Mg^{2+} ion. A similar interaction has previously been observed for K^+ ions and found to be stable in MD simulations.[35]

To study the role of fully hydrated Mg^{2+} ions in unfolding of the PK, all simulations were repeated with all the water molecules observed in the crystal structure explicitly included in the setup. This way all Mg^{2+} ions had complete hydration shells from the initial steps of the computational procedure. These setups will be referred to as the fully hydrated systems.

It should be noted that the coordination number of Mg^{2+} ions in both setups remained octahedral; only the number of water molecules in the first hydration shell is different since in the partially hydrated Mg^{2+} setup one or two water molecules are replaced by atoms of the PK, either nucleic bases or phosphate groups.

SMD stretching was performed for the following conditions: (A) WT, Mg^{2+}, C8 protonated; (B) WT, Mg^{2+}, C8 neutral; (C) WT, no Mg^{2+}, C8 protonated; (D) WT, no Mg^{2+}, C8 neutral; and (E) C8U, Mg^{2+}.

While stretching with optical tweezers was near or at equilibrium, pulling speeds in SMD were 5 m/s, several orders of magnitude larger than in the OT experimental setup, precluding any quantitative comparison of results obtained by either method. Completely stretching the PK required 3.5 ns of SMD simulation. See Supporting Information for additional details. Figures showing the PK structures were made with VMD.[36]

RESULTS

Unfolding of the BWYV PK by Optical Tweezers. Figure 1 shows typical examples of unfolding and refolding data for the wild-type (WT) PK at pH = 6.3 and pH = 7.3 and in the absence of Mg^{2+} ions. We found that a single molecule exhibited unfolding and refolding transitions both near equilibrium and off equilibrium upon consecutive stretching cycles. Unfolding and refolding parameters have been summarized in Table 1. In the case of the WT PK, pH not only affected the magnitude of the equilibrium unfolding/refolding force while leaving the nonequilibrium force unaffected but also changed the ratio of nonequilibrium versus equilibrium behaviors. Interestingly, the nonequilibrium unfolding forces proved largely the same for all WT and mutant PKs. At pH = 7.3, unfolding and refolding is almost completely near equilibrium (93%). Although the unfolding force and change in contour length differ, the ΔG° values are within experimental error, 47.8 ± 2.1 kJ/mol and 45.3 ± 3.5 kJ/mol at pH = 7.3 and 6.3, respectively.

When constructs for stretching were prepared in the absence of Mg^{2+} ions, no unfolding was ever observed in three times as many trials as the wild type with Mg^{2+} cases above. On the other hand, when constructs were prepared with Mg^{2+} ions (10 mM) but stretched in its absence, the unfolding was as in the presence of Mg^{2+} ions, indicating that Mg^{2+} ions remain associated with the unfolded PK.

We next unfolded the C8U (Figure 2A,B) and C8A (Figure 2C,D) mutants (at pH = 7.3) that affect the quadruplex base interactions thought to be essential for structural stability and shown to diminish FS efficiencies to background levels. Both

Table 1. Summary of OT Unfolding Parameters[a]

	WT, pH 6.3		WT, pH 7.3		C8U		C8A	
	equil	nonequil	equil	nonequil	equil	nonequil	equil	nonequil
F_u (pN)	15.6 ± 0.8 (55)[b]	12.9 ± 0.8 (17)	19.6 ± 0.4 (88)	13.4 ± 2.2 (3)	16.7 ± 0.4 (16)	13.6 ± 1.1 (24)	10.9 ± 0.6 (39)	13.7 ± 1.1 (24)
F_r (pN)	16.2 ± 0.9 (48)	6.3 ± 0.9 (2)	18.8 ± 0.5 (86)		16.4 ± 0.4 (14)	11.9 ± 2.4 (6)	10.5 ± 0.6 (37)	17.0 ± 3.9 (3)
$\Delta L_{c,u}$ (nts)	19 ± 1 (55)	22 ± 1 (17)	14 ± 0.3 (88)	14 ± 1 (3)	21 ± 0.1 (16)	21 ± 1 (24)	19 ± 0.9 (39)	19 ± 1 (24)
$\Delta L_{c,r}$ (nts)	18 ± 1 (48)	22 ± 1 (17)	14 ± 0.3 (86)		19 ± 1 (14)	20 ± 1 (6)	17 ± 0.9 (37)	16 ± 3 (3)
ΔG° (kJ/mol)	45.3 ± 3.5 (103)		47.8 ± 2.1 (174)		56.5 ± 2.5 (30)		26.2 ± 2.6 (76)	
%	59	41	93	7	32	68	43	57

[a] F_u, unfolding force; F_r, refolding force; $\Delta L_{c,u}$, contour length increase upon unfolding; $\Delta L_{c,r}$, contour length decrease upon refolding; ΔG°, free energy at zero force; %, percentage of stretching−relaxation cycles. [b] Number of events/transitions is given in parentheses.

dx.doi.org/10.1021/ja111281f | J. Am. Chem. Soc. 2011, 133, 9775–9782

mutants show unfolding and refolding that appears to be near equilibrium (Figure 2A,C). However, repeated unfolding and refolding, apparent as an increase in fluctuations in the force extension curve, occurs over a range of forces, in contrast with the sharp transitions observed in WT (Figure 1) and the C8U, C8A nonequilibrium data (Figure 2B,D). The C8U mutant exhibits equilibrium-type behavior less frequently than the WT PK (32%). Furthermore, the near-equilibrium parameters, unfolding/refolding force, and changes in contour length proved similar to those found with the WT at pH = 6.3. The differences in these parameters suffice, however, to yield a ΔG° = 56.5 ± 2.5 kJ/mol, which is higher than WT Refolding in the case of the nonequilibrium trajectories proved to be slow, as only six refolding events were observed among all nonequilibrium data (Table 1).

The C8A mutant shows a considerable drop in unfolding and refolding forces, which are ~11.3 pN, compared to the WT. Nonequilibrium unfolding forces were close to WT. Furthermore, only three refolding events were observed among all nonequilibrium data. The free-energy change upon unfolding/refolding derived from the near-equilibrium data equals ΔG° = 26.2 ± 2.6 kJ/mol.

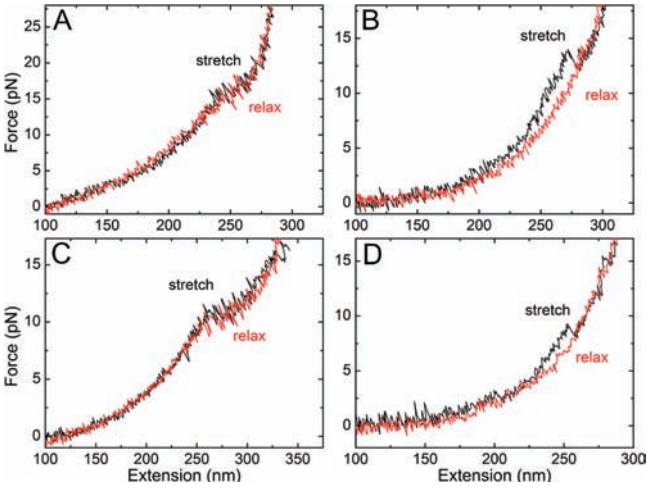

Figure 2. Typical OT force−extension data for C8U and C8A mutants. (A) Near-equilibrium and (B) off-equilibrium unfolding behavior of C8U. (C) Near-equilibrium and (D) off-equilibrium unfolding behavior of C8A.

Unfolding by SMD Simulations. The initial protocol of minimization, heating, and equilibration resulted in some structural changes of the nucleic acid backbone with respect to the crystallographic structure (see Supporting Information for detailed information about the initial preparation). For all cases, the structure of the BWYV PK preserved its characteristic fold (Figure 3 and Figure S1 in Supporting Information). However, the quadruple region in the neutral C8 system with partially hydrated Mg^{2+} ions was significantly distorted compared to the crystal structure or equilibrated structures of the other systems (Figure 3). These observations are in agreement with previous MD simulations of BWYV PK by Csaszar et al,.[30] who found that WT BWYV is generally very stable but when C8 is neutral, the quadruple region is significantly distorted. It should be noted that, in the systems where Mg^{2+} ions were partially hydrated, Mg45 changed its position and was shifted toward the quadruple with respect to the crystal structure upon equilibration (Figure 3). Further, when C8 was mutated to U8, interactions between negatively charged oxygen O4 of U8 and Mg45 caused the ion to move toward the nucleic base of U8. Displacement of Mg45 affected the position of Mg52 (Figure S2 in Supporting Information), potentially affecting the stability of stem 1 (see Discussion).

The averaged force−extension curves were computed from three SMD simulations for each of the studied systems. Figure 4 panels A and B show the individual and averaged force−extension data for the system containing partially and fully hydrated Mg^{2+} ions, respectively. In all cases the forces steadily increased early in the simulation, reaching the first maximum at an extension of 50−60 Å. The second maximum appeared at an extension of about 90 Å for the WT structure with protonated C8 (Mg^{2+} ions partially and fully hydrated) and neutral C8 (Mg^{2+} ions partially hydrated). Interestingly, the C8U mutant known to abolish −1FS[12] and the WT in the absence of Mg^{2+} ions (Figure S3, Supporting Information) lack this second force maximum. Therefore, the second force maximum may serve as a sufficient fingerprint for −1FS. Simulations in the absence of Mg^{2+} ions were not further analyzed.

Upon comparison of the unfolding trajectories with the force−extension curve, the initial increase in force appears due to friction between water and PK and due to strain arising from resistance of the PK to unfolding. The first force maximum and

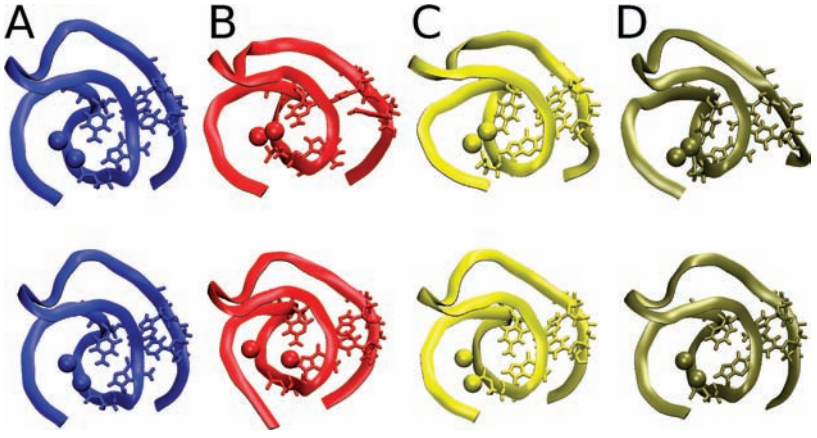

Figure 3. Comparison of initial SMD structures of the PK in various setups. (A) Crystal structure, (B) neutral C8, (C) protonated C8, and (D) C8U mutation. Top and bottom rows depict structures from the systems with partially and fully hydrated Mg^{2+} ions, respectively. Spheres denote Mg45 and Mg52 ions.

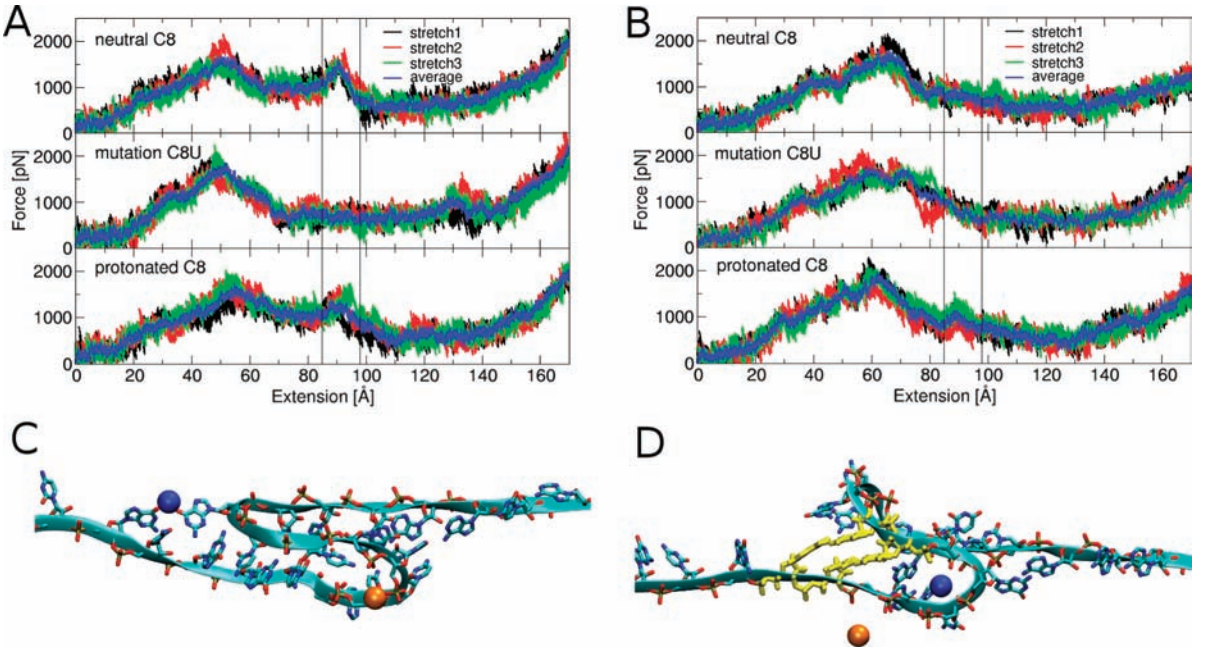

Figure 4. Individual and average force profiles from SMD simulations for systems with (A) partially and (B) fully hydrated Mg^{2+} ions. Black vertical lines at 85 and 98 Å of extension are drawn to guide eyes for easier identification of the region in the force−extension profile where the second peak occurs. Also shown are snapshots captured at the extension where the maximum of the second peak is located for the systems with (C) partially and (D) fully hydrated Mg^{2+} ions. Residues in yellow in panel D denote the new base pairing that occurred upon unfolding of the PK. Spheres denote Mg52 (blue) and Mg45 (orange) ions.

subsequent drop in force correlate with breakage of the hydrogen bonds and unfolding of stem 2, whereas the second force maximum and subsequent drop in force can be attributed to unfolding of stem 1. However, the precise unfolding mechanism of stem 1 depends upon the hydration state of the Mg^{2+} ions involved (Figure 4C,D). When Mg^{2+} ions are partially hydrated, stem 1 is stabilized by Mg52, which forms a salt bridge between bases G4 and G16 (e.g., Figure S5A, Supporting Information). Alternatively, in the fully hydrated case, stem 1 appears to be stabilized by base pairing between G7 and C15 (Watson−Crick) and between the protonated C8 and C14 (Hoogsteen). It should be noted that this is not native WT pairing (Figure S5B, Supporting Information). The newly formed base pairs are a direct result of the relative motion of the two strands of stem 1 upon stretching. It should also be noted that the second force maximum has diminished when C8 is neutral, that is, no longer protonated (Figure 4B), which decreases the ability of cytosine to form any Hoogsteen pairs. Schematic diagrams showing the two mechanisms are depicted in Figure S6 (Supporting Information). Additionally, movies based on trajectories from the SMD stretching can be downloaded from the Supporting Information.

Other short-lived interactions that are formed near the occurrence of the second force maximum were also observed: most notably, direct or water-mediated interactions of nucleic acid bases (atoms O6 from guanine and N6 from adenine) with the Mg^{2+} ion at the center of loop 1, and instantaneous weak noncomplementary base pairing between adjacent strands of stem 2 sliding over each other during the stretching. However, these interactions differed from simulation to simulation and could not be correlated with any distinct events in the force−extension curve.

The SMD trajectory also reveals the indispensible role of Mg^{2+} ions for the stability of the PK. However, the SMD simulations with either partially or fully hydrated Mg^{2+} ions show two different mechanisms of Mg^{2+} ions stabilizing stem 1, increasing its resistance to stretching. In the partially hydrated setup Mg45 was always found at the center of loop 1 interacting with phosphate groups. Such positioning of Mg45 stabilizes the turn of loop 1 and, as a result, the parallel orientation of the two strands in stem 1. In the WT structure, Mg52 formed a salt bridge between residues G4 and G16, while in the C8U mutant this salt bridge never materialized due to slight displacement of Mg45 and Mg52. In the fully hydrated setups, either Mg45 or Mg52 was found to stabilize stem 1 by entering the center of loop 1. Whenever either Mg45 or Mg52 was found to occupy the center of loop 1, the other was found to be still associated with the PK but not involved in any interaction that contributes to the resistance of the PK against stretching and unfolding. Trajectories for the C8U system revealed no characteristic structural changes of the PK that could be correlated with the force profiles. Unfolding of the mutated PK proceeded along different pathways in each SMD simulation. It has also been found that, in two out of three SMD simulations of the C8U mutant, no Mg^{2+} ions were located at the center of loop 1 at an extension of about 90 Å. This caused this loop to be less stable and resulted in easier disruption of stem 1. It is not entirely clear why none of the Mg^{2+} ions took position at the center of loop 1, but it should be noted that in all simulations with the C8U mutated PK, Mg^{2+} ions were slightly displaced in the initial structure for SMD simulations, compared to the other studied systems. It is worth noting that in one simulation the position of U8 prevented Mg45 from moving toward the center of loop 1.

■ DISCUSSION

With all our constructs unfolded with OT, we observed both near-equilibrium as well as distinct nonequilibrium behavior.

A single molecule showed both behaviors, indicating that one and the same molecule may unfold and refold along different pathways upon consecutive stretches/relaxations. Interestingly at pH = 7.3, almost all transitions for the WT PK were near equilibrium. This seems to suggest that tertiary interactions were already disrupted and that we primarily observed the unfolding of secondary structure, since tertiary interactions generally give rise to hysteresis in the force versus extension curve upon stretching and relaxation.[18,37,38] The observed increase in contour length was ~14 nucleotides (nts), considerably shorter than full PK length (26 nts) but consistent with the contour length of stem 1/loop 1. The $\Delta G°$ derived from the WT pH = 7.3 data was 45.3 ± 3.5 kJ, consistent with thermal melting data of stem 1/loop 1 by Nixon and Giedroc[17] (44.7 ± 1.3 kJ at 25 °C). Furthermore, when entering the BWYV sequence in mFold,[39,40] only residues 3−18 (stem 1/loop 1) are predicted to form secondary structure with a $\Delta G°$ of 39 kJ/mol (25 °C, 1 M NaCl, but no divalent ions). Although care should be taken in interpreting mFold data in this context—for example, the entropic states of the stretched and thermally melted structures differ—they do suggest stem 1 to unfold last, appearing as a second force maximum in the force−extension data of the SMD simulations. Since the C8U mutant, known to abolish −1FS, lacks the second force peak, one may conclude that stability of stem 1 is correlated with −1FS. Supporting this is that the pH = 7.3 data, which show unfolding of solely stem 1, best approach −1FS assay conditions. Finally, stem 1 is toward the 5′ terminus and the first structural element encountered by a translating ribosome. It is worth noting that the unfolding of solely stem 1 stands out from the WT pH = 6.3 and the C8A and C8U mutants (Table 1). The larger increase in contour lengths for the latter suggest that the PK structures, although similarly folded, may unfold along different pathways depending upon sequence (or pH), as shown by Cho et al.[41]

The SMD simulations show that, in the absence of Mg^{2+} ions, the second force peak at 90 Å extension disappeared (Figure S3, Supporting Information), which coincides with the lack of any unfolding transitions observed with OT in the absence of Mg^{2+} ions. Upon unfolding, Mg^{2+} ions remained associated with the PK primary structure as indicated by the SMD simulations and as observed with PKs prepared in the presence but stretched in the absence of Mg^{2+} ions.

Unfolding experiments with OT have suggested a correlation between the unfolding force and −1FS efficiency.[37,38,42] In interpreting our OT data in this context, the question arises whether C8 is protonated or neutral during −1FS and unfolding. Nixon and Giedroc[17] estimated the pK_a to be ~6.8, whereas Soto et al.[43] distinguished the native folded (pK_a ~ 8.2) and the first unfolded state in which noncanonical hydrogen bonding is disrupted (pK_a ~ 6.6). A similar analysis yielded a pK_a of the native folded state of ~7.8 for the data by Nixon and Giedroc[17] The OT data at pH = 7.3 therefore are consistent with a scenario in which a relatively low force disrupts noncanonical hydrogen bonding, thus lowering the pK_a well below 7.3, rendering C8 neutral, and resulting in the observation of unfolding solely the secondary structure of stem 1. This is in agreement with the predominant near equilibrium unfolding of stem 1 as expected when most tertiary interactions have been eliminated. Simple RNA and DNA hairpin structures display equilibrium unfolding behavior, in contrast to tertiary structural elements that give rise to nonequilibrium behavior as displayed by hysteresis in the folding and refolding forces.[18,37,38] It is interesting that the C8U and C8A mutants do not display the same behavior at pH = 7.3 as the WT. Increases in contour lengths upon unfolding the mutants appear similar to the WT at pH = 6.3, suggesting different unfolding pathways for the mutants and pointing to the special role and unique properties of C8. It is worth noting that the pK_a of C8 has also been proposed to approach 10−13,[44] suggesting that C8 is likely protonated in vivo and in all our OT experiments. However, if such were the case, one would have expected similar unfolding behavior of the WT in the OT experiments at both pH = 6.3 and 7.3, unless partial unfolding yields a dramatic drop in pK_a to somewhere between 6.3 and 7.3.

Although the $\Delta G°$ for the WT PK at pH = 6.3 and 7.3 were identical, a lower unfolding force was found at pH = 6.3. This is somewhat surprising, as a protonated C8 yields the possibility of an additional hydrogen bond. The equilibrated structures used for the SMD simulations show a slight rotation of the nucleic base in neutral C8, decreasing the number of possible hydrogen bonds that can be formed. With an extra hydrogen bond, one would have expected a higher rather than a lower unfolding force at pH = 6.3. Protonation at pH = 6.3 may enhance tertiary interactions, which is consistent, in a qualitative fashion, with a larger fraction of nonequilibrium transitions observed in the OT experiments. It is conceivable that disruption of such tertiary interactions by the OT more readily triggers unfolding of stem 1 and loop 1 in a perhaps more cooperative fashion, effectively lowering the required force but yielding a larger increase in contour length upon unfolding. Indeed, the increase in contour length is 19 or 22 nts at pH = 6.3 versus 14 at pH = 7.3 (see Table 1), indicating that unfolding is likely along different pathways.[41] Nixon and Giedroc[17] proposed the increased stability at low pH to be due to changes in the loop closing energetics (an entropic effect) rather than due to an increase in the number of stabilizing interactions. Therefore, our observation of a lower unfolding force may also be a consequence of the rather different entropic states of the PK in mechanical versus thermal unfolding studies. Consistent with these observations, the SMD simulations with partially hydrated Mg^{2+} ions, which mimic our entropic conditions, also show that the second force peak is higher with neutral C8. On the other hand, simulations with fully hydrated Mg^{2+} ions showed almost the opposite effect; that is, the second force maximum occurred only when C8 was protonated. We note, however, that although Mg^{2+} ions appeared fully hydrated in the crystal structure[14] and that such "diffuse" ions are thought to suffice to stabilize the PK tertiary structure,[43] it is fair to say that the hydration state of the Mg^{2+} ions remains a matter of debate and results should be considered carefully. Thus, two possible modes of interactions should be considered. Mg^{2+} ions may directly interact with nucleic bases and the backbone's phosphate groups, or they may interact via water-mediated electrostatic interaction. Both possibilities are supported by experimental and computational findings.[14,32,45−47] Therefore, two possible mechanisms explaining the second force maximum and the structural integrity of stem 1 are proposed. We note that both these mechanisms proved consistent with the −1FS efficiency assays of Kim et al.,[12] which prevented us from distinguishing between them. Furthermore, a word of caution is in order in evaluating both mechanisms because classical, pair-additive, nonpolarizable force fields such as AMBER do not accurately account for charge-related phenomena such as polarizability and charge transfer.[48]

The first mechanism is based on Mg^{2+} ions being partially hydrated (Figure 4C). Upon stretching the PK, Mg45 takes

position at the center of loop 1, which helps stabilize stem 1. Mg52 then stabilizes stem 1 by directly interacting with O6 atoms in nucleic bases of two guanine residues, G4 and G16 in stem 1. As a result, the second peak in the force profile appears. It is interesting to note that binding of potassium ion to nucleic bases in GpC sequences of RNA duplexes has been observed in computational experiments,[35] which suggests that such sites can bind positively charged ions. On the other hand, in the systems in which the salt bridge is not formed, a sudden decrease in the resistance of the PK to stretching is observed. For example, in the C8U mutant, Mg45, attracted by an oxygen atom in U8, could interact more strongly with the phosphate group of G12, which led to distortion of the backbone of the PK and then affected the orientation of the phosphate group of C13. These distortions changed the electrostatic potential around the backbone of the region C11−G12−U13, rendering it more negative toward Mg52 (see Supporting Information). As a result, Mg52 was drawn away from G4−C17 and C5−G16 (Figure S2, Supporting Information) and did not form the salt bridge stabilizing stem 1. This indirect long-range interaction between Mg45 and Mg52 resulted in the loss of the second force peak for the C8U mutant. In conclusion, unfolding of the C8U mutant with OT may still require force but may be associated with a different increase in contour length as the PK is unfolded along a different pathway.[41] Interestingly, symmetric mutations in this region, that is, from G4−C17 to C4−G17 and from C5−G16 to G5−C16, should therefore have negligible effect upon formation of the salt bridge and consequently the FS efficiency, as found by Kim et al.[12]

The second mechanism involves fully hydrated Mg^{2+} ions (Figure 4D). In this case it has been found that either Mg45 or Mg52 takes position at the center of loop 1. By interacting with negatively charged phosphate groups, such a Mg^{2+} ion stabilizes 180° turn of the loop, which stabilizes base pairing between residues in stem 1. It has been found that, in view of that mechanism, the WT with protonated C8 is unique among all the studied systems. Upon stretching, native base pairing G7−C14 and G6−C15 is replaced by another pairing of C8−C14 (Hoogsteen, possible when the C8 is protonated) and G7−C15 when the two strands of stem 1 slide one over another. Such rearrangement of the molecule when under tension increases resistance of the PK to mechanical unfolding, giving rise to the second force maximum in SMD force extension data. The C8U mutant does not exhibit the second force maximum, because with the C8U mutant no alternative base pairing can occur. Additionally, residue U8 was found to occupy the center of loop 1, effectively preventing Mg^{2+} ions from taking that position. The latter may explain why the C8G mutation also abolishes −1FS.[12] Although with C8G alternative base pairing remains a possibility, steric hindrance due to the size of the nucleic base may prevent the Mg^{2+} ion from entering the center of loop 1.

CONCLUSION

In sum, both OT experiments and SMD simulations point to the stability of BWYV PK stem 1 as being critical for −1 frameshifting, and Mg^{2+} ions proved to be essential for the stability of stem 1. Although the hydration state of the Mg^{2+} remains unclear and two different mechanisms for stabilization of stem 1 may be proposed, it is clear that changes in the positions of the Mg^{2+} ions may explain why C8 substitution mutations have much reduced FS efficiencies. In the mechanism with partially hydrated Mg^{2+} ions, the mutation affects the positions of the two Mg^{2+} ions, preventing formation of the salt bridge. In the second mechanism, with fully hydrated Mg^{2+} ions, the mutation was found to have a 2-fold effect. It prevented Mg^{2+} ions from taking position at the center of loop 1 and also disrupted the possibility of alternative base pairing in stem 1. These results suggest further mutational studies of −1FS by the BWYV, in which mutations directly affect the formation of the salt bridges or disrupt the alternative base pairing.

ASSOCIATED CONTENT

Supporting Information. Additional text with detailed experimental procedures; one table and six figures showing SMD structures and force−extension data; and four SMD movies. This material is available free of charge via the Internet at http://pubs.acs.org.

AUTHOR INFORMATION

Corresponding Author
morzech@bu.edu; visscher@physics.arizona.edu

ACKNOWLEDGMENT

M.O. thanks Piotr Cieplak from Sanford−Burnham Medical Research Institute for helpful discussion on parameter derivation for the Amber force field. We thank the University of Arizona for providing computational resources.

REFERENCES

(1) Jacks, T.; Power, M. D.; Masiarz, F. R.; Luciw, P. A.; Barr, P. J.; Varmus, H. E. *Nature* **1988**, *331*, 280–283.
(2) Jacks, T.; Madhani, H. D.; Masiarz, F. R.; Varmus, H. E. *Cell* **1988**, *55*, 447–458.
(3) Parkin, N. T.; Chamorro, M.; Varmus, H. E. *J. Virol.* **1992**, *66* (8), 5147.
(4) Yoshinaka, Y.; Katoh, I.; Copeland, T. D.; Oroszlan, S. *Proc. Natl. Acad. Sci. U. S. A.* **1985**, *82* (6), 1618.
(5) Giedroc, D. P.; Cornish, P. V. *Virus Res.* **2009**, *139*, 193–208.
(6) Plant, E. P.; Dinman, J. D. *RNA* **2006**, *12* (4), 666.
(7) Plant, E.; Jakobs, K.; Harger, J.; Meskauskas, A.; Jacobs, J.; Baxter, J.; Petrov, A.; Dinman, J. *RNA* **2003**, *9*, 168–174.
(8) Plant, E. P.; Dinman, J. D. *Nucleic Acids Res.* **2005**, *33*, 1825–1833.
(9) Namy, O.; Moran, S. J.; Stuart, D. I.; Gilbert, R. J. C.; Brierley, I. *Nature* **2006**, 244–247.
(10) Brierley, I.; Jenner, A. J.; Inglis, S. C. *J. Mol. Biol.* **1992**, *227* (2), 463.
(11) Brierley, I.; Rolley, N. J.; Jenner, A. J.; Inglis, S. C. *J. Mol. Biol.* **1991**, *220* (4), 889.
(12) Kim, Y.-G.; Su, L.; Maas, S.; O'Neill, A.; Rich, A. *Proc. Natl. Acad. Sci. U. S. A.* **1999**, *96* (25), 14234–14239.
(13) Dinman, J. D.; Wickner, R. B. *J. Virol.* **1992**, *66*, 3669–3676.
(14) Egli, M.; Minasov, G.; Su, L.; Rich, A. *Proc. Natl. Acad. Sci. U. S. A.* **2002**, *99*, 4301–4307.
(15) Egli, M.; Sarkhela, S.; Minasov, G.; Rich, A. *Helv. Chim. Acta* **2003**, *86*, 1709–1727.
(16) Su, L.; Chen, L.; Egli, M.; Berger, J. M.; Rich, A. *Nat. Struct. Biol.* **1999**, *6* (3), 285–292.
(17) Nixon, P. L.; Giedroc, D. P. *J. Mol. Biol.* **2000**, *296*, 659–671.
(18) Lipdardt, J.; Onoa, B.; Smith, S. B.; Tinoco, I., Jr.; Bustamante, C. *Science* **2001**, *292*, 733–737.
(19) Marko, J. F.; Siggia, E. D. *Macromolecules* **1995**, *28*, 8759.

(20) Wang, M. D.; Yin, H.; Landick, R.; Gelles, J.; Block, S. M. *Biophys. J.* **1997**, *72*, 1335–1346.
(21) Izrailev, F. M.; Ruffo, S.; Tessieri, L. *J Phys A: Math Theor* **1998**, *31* (23), 5263.
(22) Phillips, J. C.; Braun, R.; Wang, W.; Gumbart, J.; Tajkhorshid, E.; Villa, E.; Chipot, C.; Skeel, R. D.; Kale, L.; Schulten, K. *J. Comput. Chem.* **2005**, *26* (16), 1781.
(23) Pérez, A.; Marchán, I.; Svozil, D.; Sponer, J.; Cheatham, T. E.; Laughton, C. A.; Orozco, M. *Biophys. J.* **2007**, *92* (11), 3817.
(24) Cornell, W. D.; Cieplak, P.; Bayly, C. I.; Gould, I. R.; Merz, K. M., Jr; Ferguson, D. M.; Spellmeyer, D. C.; Fox, T.; Caldwell, J. W.; Kollman, P. A. *J. Am. Chem. Soc.* **1995**, *117* (19), 5179.
(25) Cheatham, T. E., III; Cieplak, P.; Kollman, P. A. *J. Biomol. Struct. Dyn.* **1999**, *16* (4), 845.
(26) Wang, J.; Cieplak, P.; Kollman, P. A. *J. Comput. Chem.* **2000**, *21* (12), 1049.
(27) Pearlman, D. A.; Case, D. A.; Caldwell, J. W.; Ross, W. S.; Cheatham, T. E., III; DeBolt, S.; Ferguson, D.; Seibel, G.; Kollman, P. *Comput. Phys. Commun.* **1995**, *91* (1−3), 1.
(28) Aaqvist, J. *J. Phys. Chem.* **1990**, *94* (21), 8021–8024.
(29) Varnai, P.; Zakrzewska, K. *Nucleic Acids Res.* **2004**, *32* (14), 4269–80.
(30) Csaszar, K.; Spackova, N.; Stefl, R.; Sponer, J.; Leontis, N. B. *J. Mol. Biol.* **2001**, *313* (5), 1073–91.
(31) Ohtaki, H.; Radnai, T. *Chem. Rev.* **1993**, *93* (3), 1157–1204.
(32) Bandyopadhyay, D.; Bhattacharyya, D. *J. Biomol. Struct. Dyn.* **2003**, *21*, 447–458.
(33) Sponer, J.; Burda, J. V.; Sabat, M.; Leszczynski, J.; Hobza, P. *J. Phys. Chem. A* **1998**, *102*, 5951–5957.
(34) Rulisek, L.; Sponer, J. *J. Phys. Chem. B* **2003**, *107*, 1913–1923.
(35) Auffinger, P.; Westhof, E. *J. Mol. Biol.* **2000**, *300*, 1113–1131.
(36) Humphrey, W.; Dalke, A.; Schulten, K. *J Mol Graphics* **1996**, *14*, 33–38.
(37) Green, L.; Kim, C.-H.; Bustamante, C.; I., T., Jr. *J. Mol. Biol.* **2008**, *375*, 511–528.
(38) Chen, G.; Chang, K.-Y.; Chou, M.-Y.; Bustamante, C.; Ignacio Tinoco, J. *Proc. Natl. Acad. Sci. U. S. A.* **2009**, *106* (31), 12706–12711.
(39) Zuker, M. *Nucleic Acids Res.* **2003**, *31*, 3406–15.
(40) Matthews, D. H.; Sabina, J.; Zuker, M.; Turner, D. H. *J. Mol. Biol.* **1999**, *288*, 911–940.
(41) Cho, S. S.; Pincus, D. L.; Thirumalai, D. *Proc. Natl. Acad. Sci. U. S. A.* **2009**, *106*, 17349–17354.
(42) Hansen, T.; Reihani, S.; Oddershede, L.; Sorensen, M. *Proc. Natl. Acad. Sci. U. S. A.* **2007**, *104*, 5830–5835.
(43) Soto, A. M.; Misra, V.; Draper, D. E. *Biochemistry* **2007**, *46* (11), 2973–2983.
(44) Tang, C. L.; Alexov, E.; Pyle, A. M.; Honig, H. *J. Mol. Biol.* **2007**, *366*, 1475–1496.
(45) Draper, D. E. *RNA* **2004**, *10*, 335–343.
(46) Krasovska, M. V.; Sefcikova, J.; Reblova, K.; Schneider, B.; Walter, N. G.; Sponer, J. *Biophys. J.* **2006**, *91* (2), 626.
(47) Misra, V. K.; Draper, D. E. *J. Mol. Biol.* **2000**, *299* (3), 813.
(48) McDowell, S. E.; Spackova, N.; Sponer, J.; Walter, N. G. *Biopolymers* **2007**, *85*, 169–184.